ACS OMEGA

Open Access

http://pubs.acs.org/journal/acsodf

Article

Development of a Highly Sensitive Electrochemical Sensor Using Sm_2CuZrO_6 Double Perovskite as an Electrocatalyst for Determination of Risperidone Antipsychotic Drug in Tablet Samples

Srujan Basavapura Ravikumar, Sanjay Ballur Prasanna, Nanjunda Swamy Shanthappa, Shruthi Chinnakurli Dwarakanath, Santhosh Arehalli Shivamurthy,* Sandeep Shadakshari,* Karthik Chimatahalli Shanthakumar, Hamad A. Al-lohedan, and Muthusamy Karnan

Cite This: *ACS Omega* 2023, 8, 47781−47790

Read Online

ACCESS | Metrics & More | Article Recommendations

ABSTRACT: In this study, the preparation of Sm_2CuZrO_6 double perovskites was carried out through the utilization of a sol−gel technique. The Sm_2CuZrO_6 displayed notable conductivity, impressive electrocatalytic activity, and rapid electron transfer. The monitoring of risperidone (RIS) in tablet samples is greatly influenced by these properties. Various techniques for structural and morphological characterization were employed to confirm the formation of Sm_2CuZrO_6. The electrochemical properties of Sm_2CuZrO_6 were assessed through utilization of cyclic voltammetry (CV), electrochemical impedance spectroscopy (EIS), and linear sweep voltammetry (LSV). Interestingly, the Sm_2CuZrO_6 exhibited a remarkable wide linear range of 50−500 nM, along with a detection limit of 10.62 nM. Notably, it demonstrated a sensitivity of 0.4038 $\mu A\ \mu M^{-1}\ cm^{-2}$. The constructed sensor demonstrated noteworthy selectivity, stability, and repeatability. To assess the practicality of RIS, its performance was monitored in the tablet sample, resulting in satisfactory recoveries.

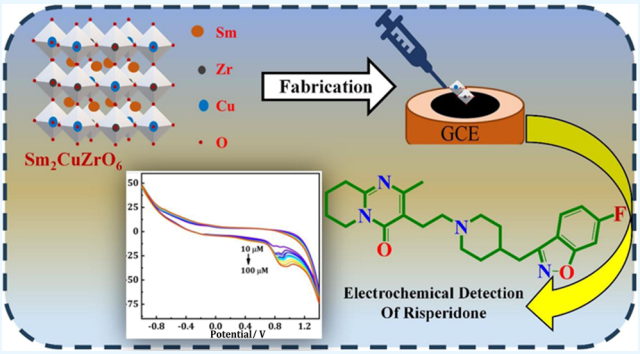

1. INTRODUCTION

Risperidone (RIS), often known as Risperdal, is a second-generation antipsychotic medication.[1] This psychoactive substance is a member of the chemical family of benzisoxazole derivatives, a potent dopamine antagonist with a significant preference for D2 dopaminergic receptors.[2,3] RIS is prescribed for various disorders, including psychotic and behavioral problems. Due to the narrow therapeutic index of RIS, its higher concentration may lead to severe toxicity and then ventricular arrhythmia, respiratory depression, seizure extrapyramidal symptoms, and so forth.[4] In this regard, it is required to develop reliable analytical methods that allow the detection of RIS in different biological fluids at broad therapeutic concentrations. Several methods were employed for RIS analysis in different media based on different techniques such as spectrophotometric methods, HPLC, electrochemical methods, chemiluminescence, etc.[5−7] Electrochemical sensing offers a multitude of advantages as a promising technique for detecting even the smallest quantities of molecules. Therefore, the development of novel sensor materials possessing electrocatalytic properties is of utmost importance to enhance the performance of present electrodes.[8−17] Consequently, we have created a cost-effective, perceptive, and sustainable monitoring technique for RIS.

Over the past few years, the scientific community has directed its attention toward double perovskite oxides, which are characterized by the chemical formula $A_2B'B''O_6$.[18] The A site may contain either a rare-earth or alkaline-earth element, while the B site's inclusion of two distinct transition-metal (TM) elements provides greater flexibility and freedom compared with a basic ABO_3 perovskite structure. The electrical properties of these oxides, which contain transition metals, are mainly influenced by the interaction between the transition-metal cations and the oxygen anions.[19] Lately, layered double perovskites, specifically $ReCuM_2O_{5+\delta}$, have garnered significant scientific interest due to their rapid oxygen-ion transport and surface exchange capabilities.[20−23] Rare earth-based double perovskites have garnered significant

Received: August 23, 2023
Revised: November 16, 2023
Accepted: November 24, 2023
Published: December 7, 2023

Scheme 1. Preparation of Synthesis of the Sm_2CuZrO_6 Double Perovskite

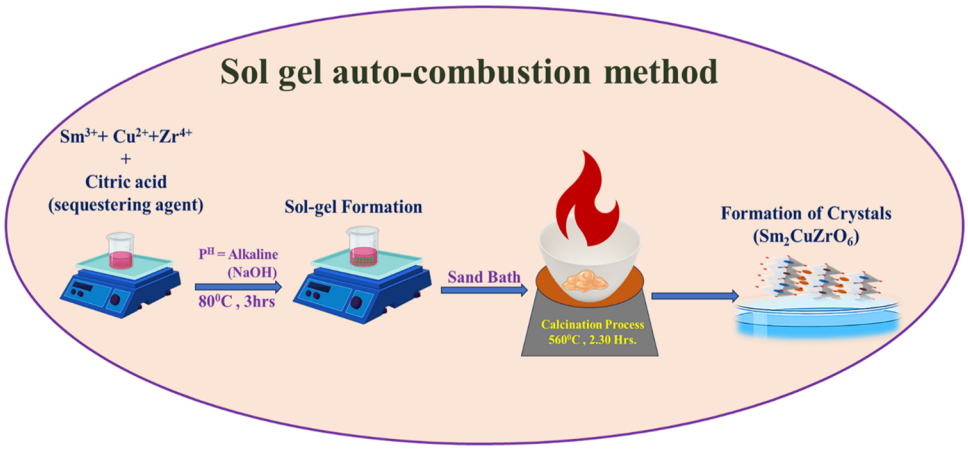

attention across various disciplines, including electrode materials, photodetectors, and supercapacitors.[24−29] Liu et al. have prepared Sr_2NiMoO_6 double perovskites using the sol−gel method and subsequently employed them as a gas sensor.[30] Durai et al. have synthesized Al_2NiCoO_5 nanoflakes for electrochemical sensing of atrazine.[31] To date, no information has been published regarding rare-earth Sm_2CuZrO_6-based double perovskites.

In the present work, we have developed highly sensitive electrochemical sensors using Sm_2CuZrO_6, a novel double perovskite compound. This rare-earth metal samarium-based compound has been effectively employed to precisely detect the antipsychotic drug Risperidone in tablet samples. It is noteworthy that the research on risperidone detection is relatively scarce, with only a limited number of articles dedicated to this topic. Our study makes a substantial contribution by successfully detecting risperidone in tablet samples using the Sm_2CuZrO_6 double perovskite sensor material. This accomplishment holds particular significance in potential overdose scenarios as it enables the identification of this antipsychotic drug. By allowing the detection of risperidone at low concentrations (50−500 nM) with a defined limit of detection (10.62 nM), our work significantly elevates the scientific relevance of this research.

2. EXPERIMENTAL SECTION

2.1. Chemicals and Reagents. The 99.9% pure samarium nitrate ($Sm(NO_3)_3$), copper nitrate ($Cu(NO_3)_2$), and zirconium nitrate ($ZrO(NO_3)_2$) were procured from Sigma-Aldrich in Mumbai, India. Utilizing $[Fe(CN)_6]^{3-/4-}$ as the electrochemical probe, the study employed a phosphate-buffered solution (PBS) consisting of 0.1 M K_2HPO_4, KH_2PO_4, and KCl. The RIS tablet sample, which was obtained from a neighborhood pharmacy, was subjected to real sample analysis. All electrochemical measurements, such as cyclic voltammetry (CV), electrochemical impedance spectroscopy (EIS), and linear sweep voltammetry (LSV), were carried out using the Versa STAT-3 instrument from Princeton Applied Research, based in the USA.

2.2. Instruments. The structural crystallinity of the synthesized material was assessed using X-ray diffraction (XRD) with the AXRD Benchtop powder diffractometer from Proto Manufacturing Limited. Thermogravimetric analysis (TGA, Q-500) and differential thermal analysis (DTG, Rigaku TG8120, Japan) determine the thermal stability of the compound. The structural morphology and elemental composition of Sm_2CuZrO_6 double perovskites were examined using scanning electron microscopy (SEM; ZEISS EVO40EP, Germany) and an energy-dispersive X-ray analysis (EDX) system connected to a transmission electron microscope (TEM; JEM 2100 F, JEOL Ltd., Japan), respectively. All electrochemical measurements were conducted using a Versa STAT-3.

2.3. Synthesis of Sm_2CuZrO_6 Double Perovskite. The sol−gel autocombustion method was employed to synthesize Sm_2CuZrO_6, a double perovskite material based on lanthanum, with citric acid acting as a sequestering agent. To obtain analytical grade precursors, a solution with a concentration of 0.05 M was prepared by dissolving carefully measured amounts of samarium nitrate ($Sm(NO_3)_3$), copper nitrate ($Cu(NO_3)_2$), and zirconium nitrate ($ZrO(NO_3)_2$) in separate beakers containing 20 mL of distilled water. A solution with a concentration of 0.3 M citric acid was created by dissolving 3.458 g of the acid in approximately 60 mL of distilled water. Each sample of metal nitrate solution was thoroughly mixed after the addition of 20 mL of the citric acid solution. The resulting solutions consist of a molar ratio of citric acid to metallic cations in a 6:1 proportion. Thoroughly mixing the three solutions of metallic nitrate and citric acid was carried out. To prevent the occurrence of precipitation, sodium hydroxide solution (NaOH) was added to the solution, thereby adjusting its pH to an alkaline level. After the solution was obtained, it underwent a gel-phase transition by being heated for 3 h at 80 °C on a magnetic stirrer. Following the acquisition of the gel, it was heated in a sand bath until complete conversion into a crystalline form was attained. The substance underwent calcination in a furnace set at 560 °C. The substance was ground into a fine powder using a mortar and pestle. The double perovskite formed is Sm_2CuZrO_6, as shown in Scheme 1, which outlines its synthesis process.

2.4. Analytical Procedure. The glassy carbon electrode (GCE) was polished with an electrode polishing kit (PK-3) before any electrode modification, resulting in a smooth surface for further modifications. The polishing procedure involved the use of aluminum and diamond slurry materials, each with a thickness of 3 mm, to effectively smooth the GCE surface. To eliminate loosely attached particles and contaminants, the polished electrode underwent multiple rounds of sonication in deionized water and was subsequently dried in a nitrogen environment. After the drying process, a 6 μL solution

https://doi.org/10.1021/acsomega.3c06254
ACS Omega 2023, 8, 47781−47790

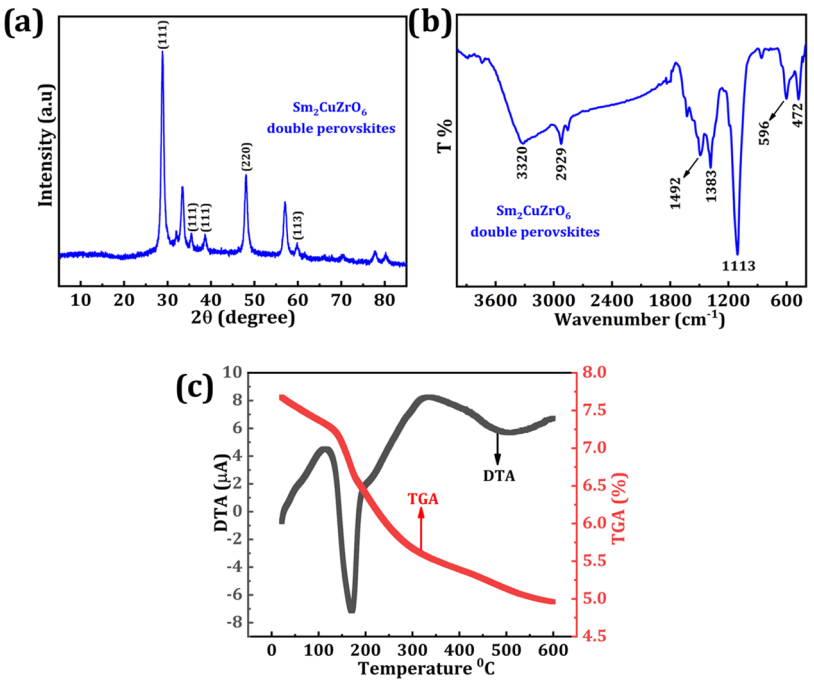

Figure 1. (a) XRD patterns, (b) FT-IR, (c) TGA, and DTA graph of the Sm_2CuZrO_6 double perovskite.

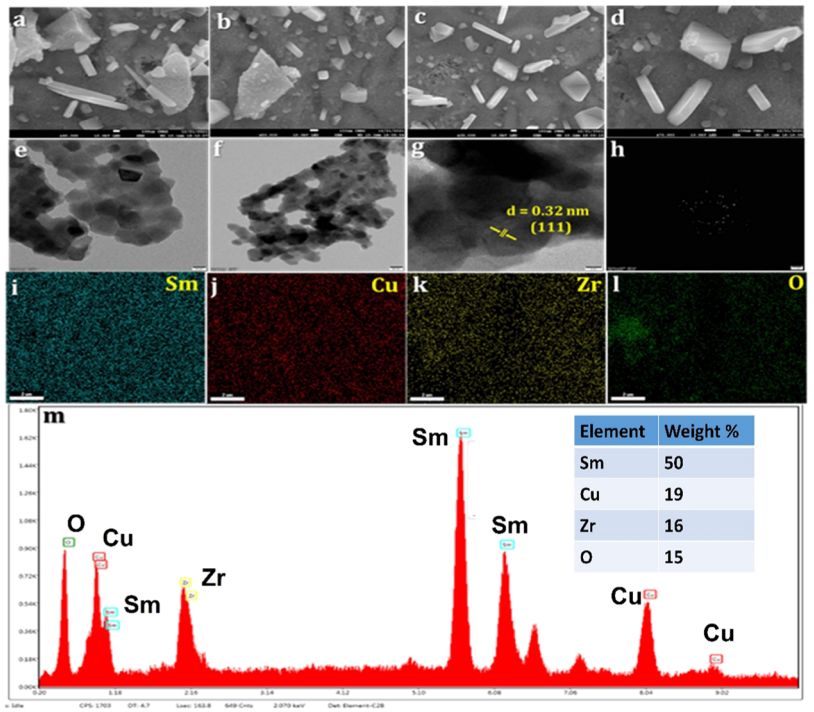

Figure 2. (a–d) SEM, (e, f) TEM, (g) HRTEM images, and (h) SAED pattern of Zn–Al LDHs nanoparticles. Elemental mapping of (i) Sm, (j) Cu, (k) Zr, and (l) O and (m) EDX analysis in the Sm_2CuZrO_6 double perovskite.

of the synthesized Sm_2CuZrO_6 material was drop-cast onto the bare GCEs exposed surface to prepare the electrode for modification. Before this modification, the Sm_2CuZrO_6 material was pretreated with a material-to-water ratio of 1:10 and subjected to sonication to ensure proper dispersion. The modified electrode was labeled as Sm_2CuZrO_6/GCE. In the electrochemical setup, three electrodes were employed for voltammetric measurements. In the three-electrode setup, the reference electrode was a saturated calomel electrode; the counter electrode was a platinum wire; and the working electrodes were the GCEs. The electrochemical tests were conducted using a 10 mL solution of 0.1 M phosphate-buffered saline (PBS) during the experimental procedure. To ensure the detection of prominent redox peaks, a scan rate of 50 mV s^{-1} was utilized in cyclic voltammetry (CV) analysis. The voltage range spanned from −1.0 to +1.4 V. Electrochemical impedance spectroscopy (EIS) was utilized in the presence of $[Fe(CN)_6]^{3-/4-}$ to obtain noteworthy redox features.

https://doi.org/10.1021/acsomega.3c06254
ACS Omega 2023, 8, 47781−47790

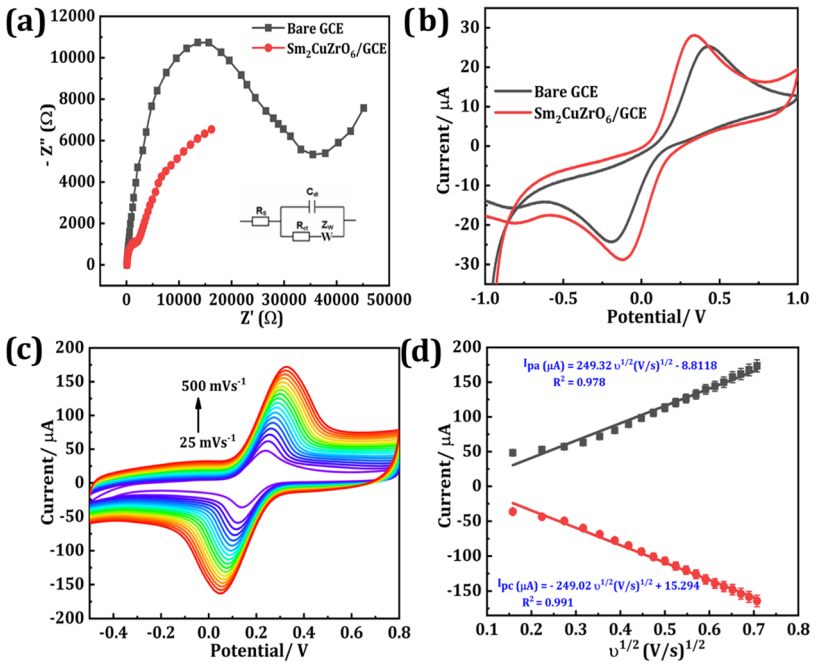

Figure 3. (a) EIS, (b) CVs spectra of bare GCE and Sm_2CuZrO_6/GCE and (a-inset) Randle's equivalent circuit image, (c) CV results at diverse υ (25−500 mV s^{-1}) in a 5 mM $[Fe(CN)_6]^{3-/4-}$ solution at Sm_2CuZrO_6/GCE and the (d) calibration plot of $\upsilon^{1/2}$ vs I_{pc} and I_{pa}.

During the execution of Linear sweep voltammetry (LSV), a pulse height of 200 mV and a pulse width of 0.05 s were used to cover a voltage range from 0.1 to 1.4 V.

3. RESULTS AND DISCUSSION

3.1. Characterizations. X-ray diffraction (XRD) is an influential method for assessing the integrity of crystal structures, providing valuable insights into the texture, orientation, size, and formation of crystallites of the prepared materials. The XRD analysis for the double perovskite Sm_2CuZrO_6 is depicted in Figure 1a. The sharp intense peaks appearing at 28.78 (2θ) (*hkl* = 111) and 48.1 (2θ) (*hkl* = 220) are perfectly identical with SmZrO, which is correlated with JCPDS Fill #01−078−1285[32] and some minimum intense peaks 2θ at 35.4 (*hkl* = 111), 38.7 (*hkl* = 111), and 59.7 (*hkl* = 113) are similar to JCPDS Fill #01−089−2529, which emphasizes the presence of CuO.[33]

The range of peaks observed in our sample Sm_2CuZrO_6 is interpreted through Fourier-transform infrared (FT-IR) analysis, as depicted in Figure 1b. FT-IR peaks around 400−600 cm^{-1} resemble the presence of CuO. The peak at 482 cm^{-1} computes CuO,[34] while the peaks from 500 to 850 cm^{-1} emphasize the presence of ZrO in the analyzed sample. 600 and 800 cm^{-1} peaks which are attributed to the Zr−O bond, thus indicating the presence of ZrO.[35] The wide intense band around 1100 to 1500 cm^{-1} shows strong adsorption, and the peaks at 1108, 1377, and 1487 cm^{-1} may be attributed to the Sm^{3+} ion.[36] The remaining broad peeks at 2936 and 3312 cm^{-1} noticed may be attributed to the weak absorption peaks, which indicate weak O−H vibrations of the moisture contents.

TGA and differential thermal analysis (DTA) were conducted over a temperature range of 20−600 °C, employing a heating rate of 5 °C min^{-1}, with a sample weighing 7.67 mg. Figure 1c reveals a two-stage thermal degradation process. The initial stage of degradation exhibited a 10% mass loss, which can be attributed to the evaporation of the moisture content present within the Sm_2CuZrO_6 double perovskite material. Subsequently, the second stage demonstrated a gradual, linear reduction in mass, indicative of material decomposition. Upon reaching the maximum temperature of 600 °C, the sample remained with a residual mass of 2.71 mg. This observation underscores the material's commendable thermal stability, demonstrating its capacity to endure high temperatures effectively.

The morphological characteristics of the Sm_2ZrCuO_6 double perovskite were thoroughly investigated by using both SEM and TEM techniques. Figure 2a−d displays the SEM images of the Sm_2CuZrO_6 double perovskite. TEM was used to determine the interior morphology of the Sm_2CuZrO_6 double perovskite. Figure 2e,f illustrates the uniform dispersion of the Sm^2CuZrO^6 double perovskite, with each particle exhibiting a characteristic flake-like morphology.

The HRTEM image of Sm_2CuZrO_6 is shown in Figure 2g. Specifically, the Sm_2CuZrO_6 (111) crystal planes are identified with *d*-spacing values of 0.32 nm. Figure 2h depicts the SAED pattern of Sm_2CuZrO_6, which is confirmed by XRD findings. The elemental mapping (Sm, Cu, Zr, and O) images of the Sm_2CuZrO_6 nanoparticles are shown in Figure 2i−l. By analysis of the energy-dispersive X-ray spectroscopy (EDS) spectra of the Sm_2CuZrO_6 material (Figure 2m), it was possible to identify the presence of different elements and quantify their elemental weight percentages (Figure 2m, inset). The results revealed that samarium accounted for 50% of the composition, followed by copper at 19%, zirconium at 16%, and oxygen at 15%. Consequently, the morphological findings substantiate the progress made in developing a Sm_2CuZrO_6 double perovskite.

3.2. Electrochemical Studies. By utilizing CV and EIS techniques, the electron transfer properties of the electrode interface in 5.0 mM $[Fe(CN)_6]^{3-/4-}$ and a scan rate of 50 mV s^{-1} were examined. In Figure 3a, the EIS spectra of the bare GCE and Sm_2CuZrO_6 double perovskite were measured, while the inset in the same figure displays an image of Randle's equivalent circuit. The R_{ct} values of 35311.43 and 2727.99 Ω

https://doi.org/10.1021/acsomega.3c06254
ACS Omega 2023, 8, 47781−47790

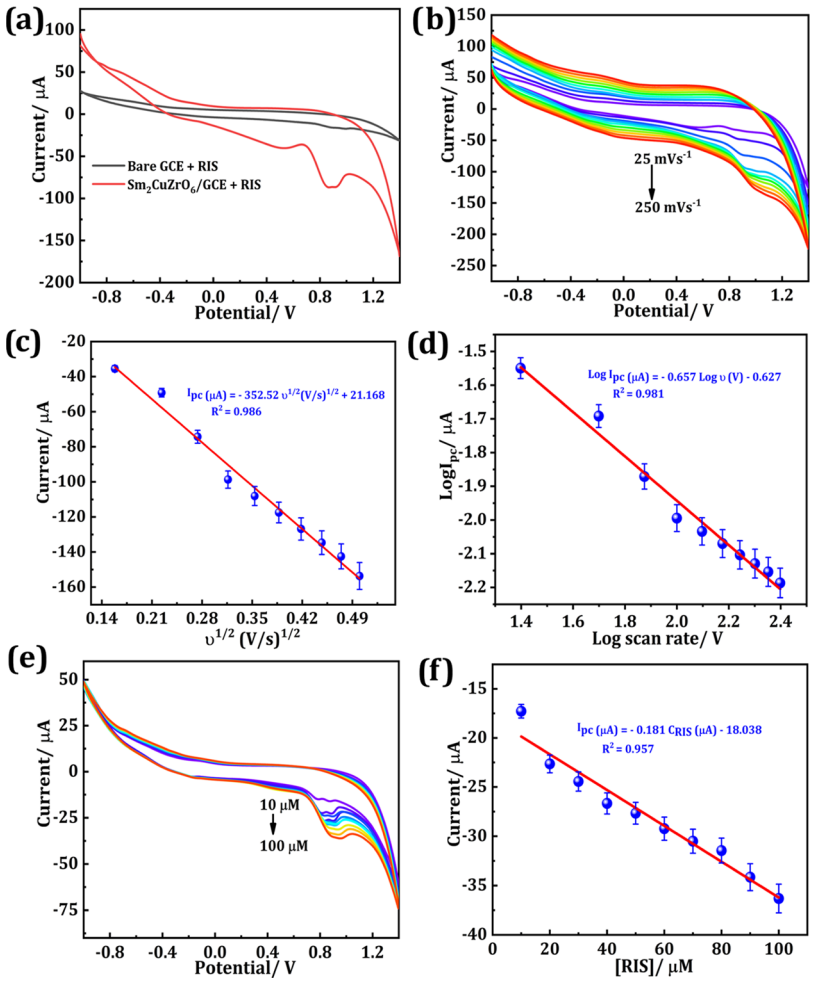

Figure 4. (a) CV spectra of bare GCE and Sm_2CuZrO_6/GCE in 100 μM RIS with 0.1 M PBS (pH 6). (b) CV curves for υ (25−250 mV s^{-1}) in 100 μM RIS and calibration plots of (c) $\upsilon^{1/2}$ $(V/s)^{1/2}$ vs I_{pc} and (d) log υ vs log I_{pc}. (e) CV responses with increasing RIS concentration (10−100 μM) on the Sm_2CuZrO_6/GCE and (f) a calibration plot.

were observed for the bare GCE and Sm_2CuZrO_6/GCE, respectively, as per the Nyquist plot analysis. Conversely, the R_{ct} of Sm_2CuZrO_6/GCE composites was significantly reduced (2727.99 Ω) due to their enhanced electron transfer efficiency and larger electrode contact areas. The electrochemical impedance spectroscopy (EIS) analysis indicated that the Sm_2CuZrO_6/GCE composite exhibited excellent conductivity and charge-transfer properties, rendering it a highly suitable material for electrochemical sensing applications.

In Figure 3b, the CV curves of bare GCE and Sm_2CuZrO_6/GCE are presented. The application of Sm_2CuZrO_6/GCE coating on GCE resulted in increased efficiency and peak currents of electron transfer compared to the GCE electrode, which suggests a faster electron transfer mechanism. An investigation was conducted to analyze the electron transfer kinetics of Sm_2CuZrO_6/GCE under varying scan rates (υ). The electrochemical properties of the Sm_2CuZrO_6/GCE are illustrated in Figure 3c, in the range of 25−500 mV s^{-1}. Notably, the I_{pa} and I_{pc} values exhibited a linear increase as υ was increased. The plot in Figure 3d illustrates the relationship between $\upsilon^{1/2}$ $(V/s)^{1/2}$ and I_{pa} and I_{pc}. The linear regression equations derived from this plot are presented as eqs 1 and 2

$$I_{pa}\ (\mu A) = 249.32\upsilon^{1/2}\ (V/s)^{1/2} - 8.8118\ (R^2 = 0.997) \quad (1)$$

$$I_{pc}\ (\mu A) = -249.02\upsilon^{1/2}\ (V/s)^{1/2} + 15.294\ (R^2 = 0.995) \quad (2)$$

The evaluation of electrode surface areas for both bare GCE and Sm_2CuZrO_6/GCE was carried out using the Randles−Sevcik equation (eq 3).

$$I_p = (2.69 \times 10^5)n^{3/2}A_0D_R^{1/2}\upsilon^{1/2}C_0 \quad (3)$$

where A = surface area, I_{pa} = oxidation peak current, n = number of electrons, D = diffusion coefficient (6×10^{-6} cm s^{-1}), and C = electrolyte concentration (5 mmol L^{-1}). The surface areas of the bare GCE and Sm_2CuZrO_6/GCE were determined to be 0.0306 and 0.0342 cm^2, respectively. The Sm_2CuZrO_6/GCE exhibited a significant electroactive surface area in the context of electrochemical sensing, offering a vast reactive site for analysis.

The electroreduction signals for the RIS are illustrated in Figure 4a, demonstrating the application of bare GCE and Sm_2CuZrO_6/GCE. On the bare GCE, the RIS reduction peak is observed at an E_{pc} of +0.91 V and I_{pc} of −17.91 μA. Remarkably, the Sm_2CuZrO_6/GCE exhibited a reduced E_{pc} and an elevated I_{pc} of +0.87 V and −87.34 μA, respectively. The electroanalytical behavior of Sm_2CuZrO_6/GCE proved to be exceptional in detecting RIS.

https://doi.org/10.1021/acsomega.3c06254
ACS Omega 2023, 8, 47781−47790

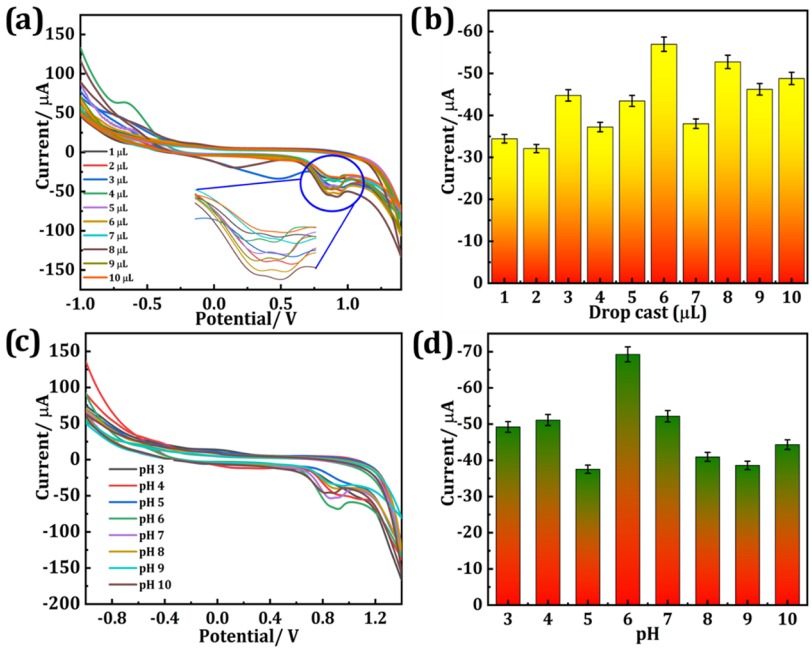

Figure 5. (a) CVs of different modifier volumes, (b) bar diagram of drop-casting volume, (c) CV response of Sm_2CuZrO_6/GCE with diverse pH values in 0.1 M PBS, and (d) pH vs I_{pc} of Sm_2CuZrO_6/GCE.

The kinetics and electron transport characteristics of Sm_2CuZrO_6/GCE were investigated by using the CV technique, with υ values being varied. The CV spectra of Sm_2CuZrO_6/GCE in 100 μM RIS with pH 6 and υ ranging from 25 to 250 mV s^{-1} are depicted in Figure 4b. As υ increases, I_{pc} demonstrates linear growth, while E_p exhibits only minimal divergence. Figure 4c illustrates the linear plot of I_{pc} versus $\upsilon^{1/2}$ $(V/s)^{1/2}$, while the regression equation (eq 4) is presented.

$$I_{pc}\ (\mu A) = -352\upsilon^{1/2}\ (V/s)^{1/2} + 21.162\ (R^2 = 0.986) \quad (4)$$

The electroreduction of RIS in Sm_2CuZrO_6/GCE was achieved through diffusion-controlled reactions. The calibration graph in Figure 4d illustrates the relationship between the logarithm of υ and the logarithm of I_{pc}, as obtained through the regression equation (eq 5) expressed as

$$\log I_{pc}\ (\mu A) = -0.657 \log \upsilon(V) - 0.627\ (R^2 = 0.981) \quad (5)$$

According to eq 5, the slope was calculated to be approximately 0.657, which closely aligns with the theoretical value of 0.5.[37] These outcomes provide additional evidence supporting the diffusion-controlled reaction of RIS.[38−41]

The electroanalytical characteristics of Sm_2CuZrO_6/GCE were examined while the concentration of RIS was varied from 10 to 100 μM. The gradual increase in RIS concentration (Figure 4e) was found to correspond with a corresponding increase in the I_{pc} values. The fast electron transfer kinetics were ascribed to the negative shift in E_{pc}, despite the increases observed with increasing RIS concentration. The calibration graph depicted in Figure 4f shows the correlation between the concentrations of RIS (μM) and the corresponding I_{pc} values. The resulting linear regression equation was derived (eq 6)

$$I_{pc}\ (\mu A) = 0.181\ C_{RIS}\ (\mu M) - 18.038\ (R^2 = 0.957) \quad (6)$$

The Sm_2CuZrO_6/GCE exhibited superior electrochemical activity for RIS sensing due to its enhanced conductivity, large surface area, electrocatalytic activity, and efficient electron transport efficiency.

3.3. Optimization of Electrochemical Studies. Figure 5a illustrates the optimization of various experimental factors for RIS detection. The drop-casting volume of Sm_2CuZrO_6/GCE on the GCE was varied from 1 to 10 μL to determine the ideal volume for the RIS analysis. The experiment involved drop-casting from 1 to 10 μL, and it was observed that the I_{pc} increased as the volume was enhanced to 6 and 7 μL. However, the I_{pc} response declined rapidly thereafter, as depicted in Figure 5b. The I_{pc} value reached its maximum at −56.97 μA when a 6 μL volume of Sm_2CuZrO_6/GCE was used. Consequently, the determination of the optimal volume for RIS sensing resulted in 6 μL of Sm_2CuZrO_6/GCE being identified as the most suitable amount.

The pH had an impact on the peak shapes, E_{pa} and I_{pa}, of the electrodes. Additionally, the ratio of protons to electrons can have a substantial impact on the reactions occurring at the electrodes. The response of Sm_2CuZrO_6/GCE to 100 μM RIS at different pH values can be observed in Figure 5c. The I_{pc} values exhibited a linear decrease with the increase in pH from 3 to 10. The maximum I_{pc} was aimed at being achieved by opting for a supporting electrolyte with a pH of 6. The electroreduction of RIS was observed to be optimal at a pH of 6. Figure 5d exhibits bar graphs illustrating the relationship between I_{pc} and various pH levels.

3.4. RIS Detection by LSV. The LSV approach is known for its superior sensitivity and selectivity in comparison to those of other electroanalytical methods. Figure 6a illustrates the electrochemical signal representing the concentration of RIS in the Sm_2CuZrO_6/GCE. The Sm_2CuZrO_6/GCE demonstrates exceptional electrocatalytic properties, as evidenced by the significant increase in LSV signals at 0.96 V with varying RIS concentrations (50 to 500 nM). A linear fit was determined by analyzing the plot of the RIS concentration

https://doi.org/10.1021/acsomega.3c06254
ACS Omega 2023, 8, 47781−47790

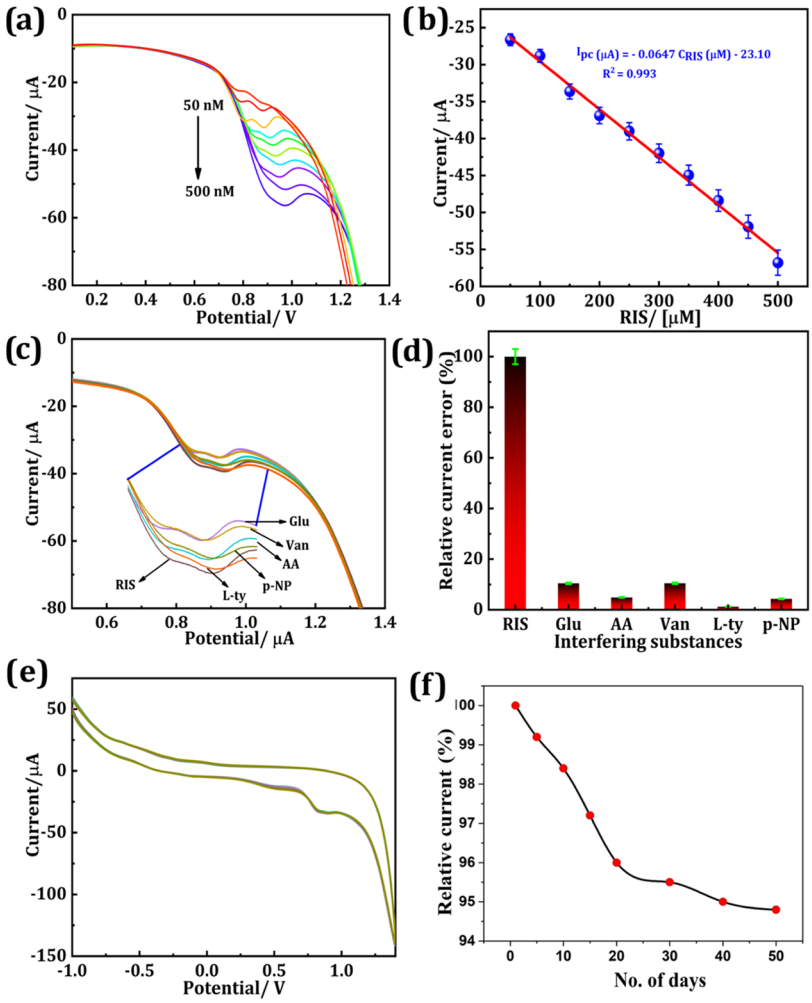

Figure 6. (a) LSV signals of Sm_2CuZrO_6/GCE for diverse concentration additions of RIS with pH 6. (b) RIS concentrations plotted with I_{pc}. (c) LSV signals for the addition of RIS with interferents. (d) Interfering substances with relative current error (%), (e) repeatability, and (f) storage stability.

Table 1. Electrochemical Reduction of RIS Was Examined Using Sm_2CuZrO_6/GCE in Comparison to Those of Various Other Materials

electrode material	method	pH	linear range (μM)	LOD (nM)	references
poly[MImEO$_8$BS]-Ni/GCE	SWV	8	0.5−80.0	73.0	42
MWCNTs/CPE	DPV	9	40−1000	12.0	43
OPPF$_6$-MWCNTs/GCE	DPV	4	0.01−0.2	6.54	44
SWCNTsCOOH-CME	DPV	8.5	0.15−15 mg L^{-1}	0.1 mg L^{-1}	45
Sm_2CuZrO_6/GCE	LSV	6	0.05−0.5	10.62	present work

(Figure 6b) with respect to I_{pc}. The linear ranges from 10 to 100 nM are represented by the eq 7

$$I_{pc}\ (\mu A) = -0.0647\ C_{RIS}\ (\mu A) - 23.10\ (R^2 = 0.993) \quad (7)$$

A sensitivity of 0.4038 μA μM^{-1} cm^{-2} was observed, along with an LOD of 10.62 nM. The incorporation of Sm_2CuZrO_6/GCE enhances the electrode's electrical conductivity. Consequently, the modified electrodes of Sm_2CuZrO_6/GCE exhibit superior electrochemical performance compared to others. In comparison to the previous RIS results (Table 1), the Sm_2CuZrO_6/GCE results showcased remarkable performance, surpassing other existing detection materials in terms of effectiveness.

3.5. Selectivity, Repeatability, and Storage Stability.

The detection of biological molecules requires a high degree of selectivity. To inspect the selectivity of RIS detection with different interfering species, LSV signals were obtained by adding 200 μM of glucose (Glu), vaniline (Van), ascorbic acid (AA), p-nitrophenol, and L-tyrosine to a solution containing 50 μM of RIS (Figure 6c). According to the LSV results, the aforementioned interfering species did not have a significant effect on the RIS signal. A bar chart (Figure 6d) illustrates the effects of interfering species on the current changes. The measured RE was under 10%, designating that the species was selected despite interference from other species.

In addition, a single Sm_2CuZrO_6/GCE was used to examine repeatability (Figure 6e). An RSD value of 2.89% was achieved, indicating that Sm_2CuZrO_6/GCE had acceptable repeatability.

https://doi.org/10.1021/acsomega.3c06254
ACS Omega 2023, 8, 47781−47790

The Sm_2CuZrO_6/GCE was kept in a refrigerator for 50 days to investigate its storage stability. Figure 6f depicts the LSV signals for storage stability in the time period of 1 to 50 days. It shows that 94.74% of the initial value is retained after 50 days of storage. Based on these results, Sm_2CuZrO_6/GCE exhibited excellent stability for detecting RIS.

3.6. Real Sample Analysis. To evaluate the analytical applicability of the proposed method, it was also employed in the determination of risperidone in tablets (tablets containing 2 mg). The results for the determination of risperidone are presented in Table 2. Satisfactory recoveries of the experimental results were determined for risperidone.

Table 2. Determination of RIS in Tablet Samples Using the Sm_2CuZrO_6/GCE Sensor

tablet samples	added (nM) (n = 3)	found (nM)	recovery (%)	RSD (%)
risperidone	10	9.74	97.4	4.16
	20	19.57	97.85	3.74
	30	28.44	94.8	3.99

4. CONCLUSIONS

In this study, a novel electrochemical sensor based on Sm_2CuZrO_6 double perovskites was synthesized by the sol–gel method. The sensor exhibited an excellent electrocatalytic response for RIS sensing. The Sm_2CuZrO_6/GCE indicated the electroreduction of RIS in tablet samples. In addition, the LSV response of the sensor showed good linearity in the range of 50–500 nM with a LOD of 10.62 nM and sensitivity of 0.4038 $\mu A\ \mu M^{-1}\ cm^{-2}$. The higher sensitivity of the RIS sensor was attributed to the good conducting ability, large surface area, and enhanced catalytic activity of the Sm_2CuZrO_6 double perovskite. Moreover, Sm_2CuZrO_6/GCE exhibited appreciable selectivity, storage stability, and repeatability. The practicability of Sm_2CuZrO_6/GCE was evaluated by monitoring RIS in tablet samples, and the results showed good recoveries. This newly developed sensor shows promise for detecting RIS in pharmaceutical tablet samples.

AUTHOR INFORMATION

Corresponding Authors

Santhosh Arehalli Shivamurthy – *Department of Chemistry (U.G.), N.M.K.R.V. College for Women, Bangalore, Karnataka 560011, India;* orcid.org/0000-0002-6606-3026; Phone: +91 8861027395; Email: santhu41100@gmail.com

Sandeep Shadakshari – *Department of Chemistry, SJCE, JSS Science and Technology University, Mysuru, Karnataka 570006, India;* orcid.org/0000-0003-4342-4623; Phone: +91 9591572962; Email: sandeep12chem@gmail.com

Authors

Srujan Basavapura Ravikumar – *Department of Chemistry, SJCE, JSS Science and Technology University, Mysuru, Karnataka 570006, India*

Sanjay Ballur Prasanna – *Department of Chemical Engineering and Biotechnology, National Taipei University of Technology (Taipei Tech), Taipei 10608, Taiwan*

Nanjunda Swamy Shanthappa – *Department of Chemistry, SJCE, JSS Science and Technology University, Mysuru, Karnataka 570006, India*

Shruthi Chinnakurli Dwarakanath – *Department of Chemistry (U.G.), N.M.K.R.V. College for Women, Bangalore, Karnataka 560011, India*

Karthik Chimatahalli Shanthakumar – *Department of Chemistry, SJCE, JSS Science and Technology University, Mysuru, Karnataka 570006, India*

Hamad A. Al-lohedan – *Department of Chemistry, College of Science, King Saud University, Riyadh 11451, Saudi Arabia*

Muthusamy Karnan – *Grassland and Forage Division, National Institute of Animal Science, Rural Development Administration, Cheonan, Chungcheongnam-do 3100, South Korea*

Complete contact information is available at: https://pubs.acs.org/10.1021/acsomega.3c06254

Author Contributions

S.B.R.: writing—original draft, writing—review and editing, methodology, formal analysis, data curation, and visualization. S.B.P.: writing—review and editing. S.C. and N.S.S.: writing—review and editing and methodology. H.A.A.-l. and M.K. funding acquisition and methodology. S.S.: writing—review and editing and methodology. S.A.S.: conceptualization, methodology, supervision, project administration, funding acquisition, and writing—review and editing.

Notes

The authors declare no competing financial interest.

ACKNOWLEDGMENTS

The authors are grateful for the financial support of this research from the author (Hamad A. Al-lohedan) and acknowledge Researchers Supporting Project number (RSP2023R54), King Saud University, Riyadh, Saudi Arabia.

REFERENCES

(1) Cappadocia, M. C.; Desrocher, M.; Pepler, D.; Schroeder, J. H. Contextualizing the Neurobiology of Conduct Disorder in an Emotion Dysregulation Framework. *Clin. Psychol. Rev.* **2009**, *29* (6), 506–518.

(2) Riva, R.; Banfi, L.; Castaldi, G.; Ghislieri, D.; Malpezzi, L.; Musumeci, F.; Tufaro, R.; Rasparini, M. Selective Chemical Oxidation of Risperidone: A Straightforward and Cost-Effective Synthesis of Paliperidone. *Eur. J. Org. Chem.* **2011**, *2011* (12), 2319–2325.

(3) Avenoso, A.; Facciolà, G.; Salemi, M.; Spina, E. Determination of Risperidone and Its Major Metabolite 9-Hydroxyrisperidone in Human Plasma by Reversed-Phase Liquid Chromatography with Ultraviolet Detection. *J. Chromatogr. B: Biomed. Sci. Appl.* **2000**, *746* (2), 173–181.

(4) Jerrell, J. M.; McIntyre, R. S.; Tripathi, A. Childhood Treatment with Psychotropic Medication and Development of Comorbid Medical Conditions in Adolescent-Onset Bipolar Disorder. *Hum. Psychopharmacol.: Clin. Exp.* **2011**, *26* (7), 451–459.

(5) Peng, J.; Huang, Q.; Zhuge, W.; Liu, Y.; Zhang, C.; Yang, W.; Xiang, G. Blue-Light Photoelectrochemical Sensor Based on Nickel Tetra-Amined Phthalocyanine-Graphene Oxide Covalent Compound for Ultrasensitive Detection of Erythromycin. *Biosens. Bioelectron.* **2018**, *106*, 212–218.

(6) Peng, J.; Huang, Q.; Liu, Y.; Liu, P.; Zhang, C. Photoelectrochemical Sensor Based on Composite of CdTe and Nickel Tetra-Amined Phthalocyanine Covalently Linked with Graphene Oxide for Ultrasensitive Detection of Curcumin. *Sens. Actuators, B* **2019**, *294*, 157–165.

https://doi.org/10.1021/acsomega.3c06254
ACS Omega 2023, 8, 47781–47790

(7) Peng, J.; Li, X.; Liu, Y.; Zhuge, W.; Zhang, C.; Huang, Y. Photoelectrochemical Sensor Based on Zinc Phthalocyanine Semiconducting Polymer Dots for Ultrasensitive Detection of Dopamine. *Sens. Actuators, B* **2022**, *360*, No. 131619, DOI: 10.1016/j.snb.2022.131619.
(8) Darabi, R.; Shabani-Nooshabadi, M. NiFe2O4-RGO/Ionic Liquid Modified Carbon Paste Electrode: An Amplified Electrochemical Sensitive Sensor for Determination of Sunset Yellow in the Presence of Tartrazine and Allura Red. *Food Chem.* **2021**, *339*, No. 127841.
(9) Shabani-Nooshabadi, M.; Tahernejad-Javazmi, F. Electrocatalytic Determination of Hydroxylamine in the Presence of Thiosulfate in Water and Wastewater Samples Using a Nanostructure Modified Carbon Paste Electrode. *Electroanalysis* **2015**, *27* (7), 1733−1741.
(10) Jafari, Y.; Shabani-Nooshabadi, M.; Ghoreishi, S. M. Electropolymerized Coatings of Poly(o-Anisidine) and Poly(o-Anisidine)-TiO_2 Nanocomposite on Aluminum Alloy 3004 by Using the Galvanostatic Method and Their Corrosion Protection Performance. *Polym. Adv. Technol.* **2014**, *25* (3), 279−287.
(11) Shabani-Nooshabadi, M.; Karimi-Maleh, H.; Tahernejad-Javazmi, F. Fabrication of an Electroanalytical Sensor for Determination of Deoxyepinephrine in the Presence of Uric Acid Using CuFe 2 O 4 Nanoparticle/Ionic Liquid Amplified Sensor. *J. Electrochem. Soc.* **2019**, *166* (6), H218−H223, DOI: 10.1149/2.1261906jes.
(12) Tahernejad-Javazmi, F.; Shabani-Nooshabadi, M.; Karimi-Maleh, H.; Naeimi, H. Square Wave Voltammetric Determination of Hydrazine and 4-Chlorophenol as Two Important Water Pollutants Using Nanostructure-Amplified Sensor. *Res. Chem. Intermed.* **2018**, *44* (9), 5389−5401.
(13) Tahernejad-Javazmi, F.; Shabani-Nooshabadi, M. Voltammetric Determination of Thiosulfate in Presence of P-Nitrophenol Using an Electrochemical Nanostructure Sensor Modified with a New Mediator. *J. Electrochem. Soc.* **2017**, *164* (13), H975−H980.
(14) Misaghpour, F.; Shabani-Nooshabadi, M. An Electrochemical Sensor for Analysis of Food Red 17 in the Presence of Tartrazine in Food Products Amplified with CdO/RGO Nanocomposite and 1,3-Dipropylimidazolium Bromide. *Food Anal. Methods* **2018**, *11* (3), 646−653.
(15) Tahernejad-Javazmi, F.; Shabani-Nooshabadi, M.; Karimi-Maleh, H. 3D Reduced Graphene Oxide/FeNi3-Ionic Liquid Nanocomposite Modified Sensor; an Electrical Synergic Effect for Development of Tert-Butylhydroquinone and Folic Acid Sensor. *Composites, Part B* **2019**, *172*, 666−670.
(16) Akbarian, Y.; Shabani-Nooshabadi, M.; Karimi-Maleh, H. Fabrication of a New Electrocatalytic Sensor for Determination of Diclofenac, Morphine and Mefenamic Acid Using Synergic Effect of NiO-SWCNT and 2, 4-Dimethyl-N/-[1- (2, 3-Dihydroxy Phenyl) Methylidene] Aniline. *Sens. Actuators, B* **2018**, *273*, 228−233.
(17) Cheraghi, S.; Taher, M. A.; Karimi-Maleh, H.; Karimi, F.; Shabani-Nooshabadi, M.; Alizadeh, M.; Al-Othman, A.; Erk, N.; Raman, P. K. Y.; Karaman, C. Novel Enzymatic Graphene Oxide Based Biosensor for the Detection of Glutathione in Biological Body Fluids. *Chemosphere* **2022**, *287*, No. 132187, DOI: 10.1016/j.chemosphere.2021.132187.
(18) Lavat, A. E.; Baran, E. J. IR-Spectroscopic Characterization of A2BB′O6 Perovskites. *Vib. Spectrosc.* **2003**, *32* (2), 167−174.
(19) Saha-Dasgupta, T. Magnetism in Double Perovskites. *J. Supercond. Novel Magn.* **2013**, *26* (5), 1991−1995.
(20) Chen, Y.; deGlee, B.; Tang, Y.; Wang, Z.; Zhao, B.; Wei, Y.; Zhang, L.; Yoo, S.; Pei, K.; Kim, J. H.; Ding, Y.; Hu, P.; Tao, F. F.; Liu, M. A Robust Fuel Cell Operated on Nearly Dry Methane at 500 °C Enabled by Synergistic Thermal Catalysis and Electrocatalysis. *Nat. Energy* **2018**, *3* (12), 1042−1050.
(21) Anjum, U.; Khan, T. S.; Agarwal, M.; Haider, M. A. Identifying the Origin of the Limiting Process in a Double Perovskite PrBa 0.5 Sr 0.5 Co 1.5 Fe 0.5 O 5+δ Thin-Film Electrode for Solid Oxide Fuel Cells. *ACS Appl. Mater. Interfaces* **2019**, *11* (28), 25243−25253.
(22) Wang, L.; Xie, P.; Bian, L.; Liu, X.; Chou, K. Performance of Ca-Doped GdBa1-XCaxFe2O5+δ(X = 0, 0.1) as Cathode Materials for IT-SOFC Application. *Catal. Today* **2018**, *318*, 132−136.
(23) Hashim, S. S.; Liang, F.; Zhou, W.; Sunarso, J. Cobalt-Free Perovskite Cathodes for Solid Oxide Fuel Cells. *ChemElectroChem* **2019**, *6* (14), 3549−3569.
(24) Raril, C.; Manjunatha, J. G. Sensitive Electrochemical Analysis of Resorcinol Using Polymer Modified Carbon Paste Electrode: A Cyclic Voltammetric Study. *Anal. Bioanal. Electrochem.* **2018**, *10* (4), 488−498.
(25) Hashisaka, M.; Kan, D.; Masuno, A.; Takano, M.; Shimakawa, Y.; Terashima, T.; Mibu, K. Epitaxial Growth of Ferromagnetic La2NiMnO6 with Ordered Double-Perovskite Structure. *Appl. Phys. Lett.* **2006**, *89* (3), No. 032504, DOI: 10.1063/1.2226997.
(26) Rajendran, D. N.; Nair, K. R.; Rao, P. P.; Sibi, K. S.; Koshy, P.; Vaidyan, V. K. New Perovskite Type Oxides: NaATiMO6 (A = Ca or Sr; M = Nb or Ta) and Their Electrical Properties. *Mater. Lett.* **2008**, *62* (4−5), 623−628, DOI: 10.1016/j.matlet.2007.06.022.
(27) Hamakawa, S.; Li, L.; Li, A.; Iglesia, E. Synthesis and Hydrogen Permeation Properties of Membranes Based on Dense SrCe0.95Yb0.05O3-α Thin Films. *Solid State Ionics* **2002**, *148* (1−2), 71−81.
(28) Yoshimatsu, K.; Nogami, K.; Watarai, K.; Horiba, K.; Kumigashira, H.; Sakata, O.; Oshima, T.; Ohtomo, A. Synthesis and Magnetic Properties of Double-Perovskite Oxide La 2 MnFeO 6 Thin Films. *Phys. Rev. B* **2015**, *91*, No. 054421, DOI: 10.1103/PhysRevB.91.054421.
(29) Meng, Z.; Xu, J.; Yu, P.; Hu, X.; Wu, Y.; Zhang, Q.; Li, Y.; Qiao, L.; Zeng, Y.; Tian, H. Double Perovskite La2CoMnO6 Hollow Spheres Prepared by Template Impregnation for High-Performance Supercapacitors. *Chem. Eng. J.* **2020**, *400*, No. 125966, DOI: 10.1016/j.cej.2020.125966.
(30) Liu, T.; Wang, T.; Li, H.; Su, J.; Hao, X.; Liu, F.; Liu, F.; Liang, X. Ethanol Sensor Using Gadolinia-Doped Ceria Solid Electrolyte and Double Perovskite Structure Sensing Material. *Sens. Actuators, B* **2021**, *349*, No. 130771, DOI: 10.1016/j.snb.2021.130771.
(31) Durai, L.; Badhulika, S. Highly Selective Trace Level Detection of Atrazine in Human Blood Samples Using Lead-Free Double Perovskite Al2NiCoO5Modified Electrode via Differential Pulse Voltammetry. *Sens. Actuators, B* **2020**, *325*, No. 128792, DOI: 10.1016/j.snb.2020.128792.
(32) Wu, S.; Xue, Z.; Ji, X.; Byon, E.; Zhang, S. Influence of Y3Al5O12 Doping on Mechanical Properties and Thermal Conductivity of Sm2Zr2O7-Y3Al5O12 Composite Ceramics. *J. Alloys Compd.* **2020**, *842*, No. 155872.
(33) Saied, M.; Hasanin, M.; Abdelghany, T. M.; Amin, B. H.; Hashem, A. H. Anticandidal Activity of Nanocomposite Based on Nanochitosan, Nanostarch and Mycosynthesized Copper Oxide Nanoparticles against Multidrug-Resistant Candida. *Int. J. Biol. Macromol.* **2023**, *242*, No. 124709.
(34) Zhang, X.; Kamali, M.; Xue, Y.; Li, S.; Costa, M. E. V.; Cabooter, D.; Dewil, R. Periodate Activation with Copper Oxide Nanomaterials for the Degradation of Ciprofloxacin - A New Insight into the Efficiency and Mechanisms. *J. Cleaner Prod.* **2023**, *383*, No. 135412.
(35) Akram, S.; Bashir, M.; Majid, F.; Ayub, M.; Khan, B. S.; Saeed, A.; Shaik, M. R.; Khan, M.; Shaik, B. Stabilization of Zirconia Nanoparticles by Collagen Protein and Calcium Carbonate Extracted from Eggshell and Its Biodegradation, Radical Scavenging and Mineralization Activity. *Arabian J. Chem.* **2023**, *16* (10), No. 105135, DOI: 10.1016/j.arabjc.2023.105135.
(36) Priya, T. S.; Nataraj, N.; Chen, T. W.; Chen, S. M.; Kokulnathan, T. Synergistic Formation of Samarium Oxide/Graphene Nanocomposite: A Functional Electrocatalyst for Carbendazim Detection. *Chemosphere* **2022**, *307*, No. 135711, DOI: 10.1016/j.chemosphere.2022.135711.
(37) Prasanna, S. B.; Sakthivel, R.; Lin, L.-Y.; Duann, Y.-F.; He, J.-H.; Liu, T.-Y.; Chung, R.-J. MOF Derived 2D-Flake-like Structured Mn 3 Co 3 O 4 Integrated Acid Functionalized MWCNT for Electrochemical Detection of Antibiotic Furazolidone in Biological

https://doi.org/10.1021/acsomega.3c06254
ACS Omega 2023, 8, 47781−47790

Fluids. *Appl. Surf. Sci.* **2022**, *611*, No. 155784, DOI: 10.1016/j.apsusc.2022.155784.
(38) Prasanna, S. B.; Lin, Y.-C.; Ramaraj, S. K.; Dhawan, U.; Liu, X.; Tung, C.-W.; Sakthivel, R.; Chung, R.-J. 2D/2D Heterostructure Ni-Fe LDH/Black Phosphorus Nanosheets with AuNP for Noxious Substance Diphenylamine Detection in Food Samples. *Food Chem.* **2024**, *432*, No. 137295.
(39) Prasanna, S. B.; Kumar, G. K. S.; Shadakshari, S.; Shivamurthy, S. A.; Shanthakumar, K. C.; Nagaraja, B. M.; Chung, R.-J. Advanced Sensing of Antibiotics with Sr@Se Flower-Like Structure on Phosphorus-Doped g-C3N4 Composite: Application towards Detection of Chloramphenicol in Food Samples. *Chemosensors* **2022**, *10* (10), No. 425, DOI: 10.3390/chemosensors10100425.
(40) Prasanna, S. B.; Bahajjaj, A. A. A.; Lee, Y.-H.; Lin, Y.-C.; Dhawan, U.; Sakthivel, R.; Chung, R.-J. Highly Responsive and Sensitive Non-Enzymatic Electrochemical Sensor for the Detection of β-NADH in Food, Environmental and Biological Samples Using AuNP on Polydopamine/Titanium Carbide Composite. *Food Chem.* **2023**, *426*, No. 136609.
(41) Prasanna, S. B.; Sakthivel, R.; Lin, L.-Y.; Duann, Y.-F.; He, J.-H.; Liu, T.-Y.; Chung, R.-J. MOF Derived 2D-Flake-like Structured Mn3Co3O4 Integrated Acid Functionalized MWCNT for Electrochemical Detection of Antibiotic Furazolidone in Biological Fluids. *Appl. Surf. Sci.* **2023**, *611*, No. 155784, DOI: 10.1016/j.apsusc.2022.155784.
(42) Molaakbari, E.; Mostafavi, A.; Tohidiyan, Z.; Beitollahi, H. Synthesis and Application of Conductive Polymeric Ionic Liquid/Ni Nanocomposite to Construct a Nanostructure Based Electrochemical Sensor for Determination of Risperidone and Methylphenidate. *J. Electroanal. Chem.* **2017**, *801*, 198−205, DOI: 10.1016/j.jelechem.2017.07.001.
(43) Afkhami, A.; Ghaedi, H. Multiwalled Carbon Nanotube Paste Electrode as an Easy, Inexpensive and Highly Selective Sensor for Voltammetric Determination of Risperidone. *Anal. Methods* **2012**, *4* (5), 1415−1420.
(44) Arvand, M.; Pourhabib, A. Adsorptive Stripping Differential Pulse Voltammetric Determination of Risperidone with a Multi-Walled Carbon Nanotube-Ionic Liquid Paste Modified Glassy Carbon Electrode. *J. Chin. Chem. Soc.* **2013**, *60*, 63−72, DOI: 10.1002/jccs.201200161.
(45) Merli, D.; Dondi, D.; Pesavento, M.; Profumo, A. Electrochemistry of Olanzapine and Risperidone at Carbon Nanotubes Modified Gold Electrode through Classical and DFT Approaches. *J. Electroanal. Chem.* **2012**, *683*, 103−111, DOI: 10.1016/j.jelechem.2012.08.011.

https://doi.org/10.1021/acsomega.3c06254
ACS Omega 2023, 8, 47781−47790